Online Optimal Tuning of Relay Feedback Controllers for a class of Second-Order Systems with Limited Measurements

Marc Hampe * **Sebastian Leonow** ** **Martin Mönnigmann** ***

* *Ruhr-Universität Bochum, Bochum, 44801 Germany (e-mail: marc.hampe@rub.de).*
** *Ruhr-Universität Bochum, Bochum, 44801 Germany (e-mail: sebastian.leonow@rub.de).*
*** *Ruhr-Universität Bochum, Bochum, 44801 Germany (e-mail: martin.moennigmann@rub.de).*

Abstract:
We propose a novel, self-optimizing relay feedback control for a class of second-order systems. The proposed controller achieves a control performance that is close to that of continuous (e.g., PID) control, but it requires only very limited process information, acquired from a two-valued signal of a simple binary sensor. The smooth output of the proposed controller results in reduced energy consumption and wear of the actuator.

Keywords: Adaptive control, Second-order systems, Relay control, Process control, Discontinuous control

1. INTRODUCTION

Relay feedback controllers are used in many applications ranging from home to industrial automation systems. In particular, they are used for systems with low accuracy requirements often found in temperature, pressure, level and humidity control. Typical applications include heating, ventilation and air conditioning systems (HVAC) (e.g. Li and Alleyne, 2010). Methods for auto-tuning controllers in the process industry (e.g. Levy et al., 2012) and delta-sigma converters for audio processing (e.g. Ardalan and Paulos, 1987) are also based on relay feedback. The ability to stabilize complex systems and the simplicity of the algorithm allow for easy implementation without requiring advanced knowledge of the underlying system dynamics or control theory in general.

Numerous publications concerning stability investigations (da Silva and Barros, 2019, Feofilov and Kozyr, 2019) and optimization for common system classes (Hetel et al., 2015) and specific applications (Kang et al., 2015, Al-Azba et al., 2020, Elbert et al., 2014) stress the need for research, while several patents (Dietzel and Bek, 1996, Juntunen, 2005, Michalek, 1990) show the importance of relay feedback controllers in practical setups.

The simplicity of relay feedback entails the disadvantages of partially high-frequent oscillations around the setpoint, high stress on the actuator as well as an increased energy consumption. To address these issues we proposed an adaptive control algorithm in Leonow and Mönnigmann (2019) and Leonow et al. (2019) suited for first-order systems. The algorithm uses adapted relay parameters to reduce actuator stress and energy consumption to an extent comparable to a continuous PID-type controller. A significant limitation of the proposed controller in former publications is its restriction to first-order systems.

This paper extends the adaptive relay feedback to systems of second-order by exploiting the second-order system dynamics and, in particular, their step responses, which appear naturally during relay feedback control.

2. PRELIMINARIES

The plant of consideration can be modeled with a critically damped, second-order LTI system

$$\dot{x}(t) = \underbrace{\begin{pmatrix} 0 & 1 \\ -1/T^2 & -2/T \end{pmatrix}}_{A} x(t) + \underbrace{\begin{pmatrix} 0 \\ k/T^2 \end{pmatrix}}_{b} u(t),\ y(t) = \underbrace{(1\ 0)}_{c^T} x(t) \tag{1}$$

with input $u(t)$ and output $y(t)$. The output $y(t)$ is assumed not to be measured continuously but by a state-discrete, binary sensor with output $s(t)$, detailed further below in (2). The plant gain $k > 0$ and the time constant $T > 0$ are assumed to be unknown but constant or slowly changing ($\mathrm{d}k/\mathrm{d}t,\ \mathrm{d}T/\mathrm{d}t \ll T$). It is easy to show that A is Hurwitz under the conditions for k and T. In particular, A^{-1} exists.

We impose strong constraints on the system class to allow an autonomous parameter estimation from the very limited process information obtained with binary measurements. Moreover, these constraints ensure certain class-wide properties of the resulting limit cycles (see Sec. 3).

The binary sensor is assumed to provide a two-valued signal $s \in \{0, 1\}$

⋆ This project was supported by funds from the Europäischer Fonds für regionale Entwicklung (EFRE).

$$s(t) = \begin{cases} 1 & : (y(t) > w + h) \vee (y(t) > w - h \wedge s(t^\dagger) = 1) \\ 0 & : (y(t) < w - h) \vee (y(t) < w + h \wedge s(t^\dagger) = 0) \end{cases} . \tag{2}$$

Here, w is the sensor setpoint, $h > 0$ is the sensor hysteresis and $t^\dagger$ denotes a point in time immediately prior to the actual time t.

3. LIMIT CYCLES

The adaptive binary controller translates the sensor signal $s(t)$ into the plant input $u(t)$ according to

$$u(t) = \begin{cases} \mu + \delta & : s = 0 \\ \mu - \delta & : s = 1 \end{cases} , \tag{3}$$

where $\mu \in \mathbb{R}$ is the mean value and $\delta \in \mathbb{R}^{>0}$ is the amplitude. Both parameters will be adjusted with the proposed self-optimizing algorithm (see Sec. 4.5) until the optimal parameters for the specific system are found. The optimal controller parameters μ^* and δ^* fulfill the following properties:

- μ^* compensates the sensor offset w, i.e.,
$$u(t) = \mu^* \text{ yields } y(t \to \infty) \to w \text{ and} \tag{4}$$
- δ^* is the lowest amplitude that yields
$$y(t \to \infty) = w \pm h \text{ for } u(t) = \mu^* \pm \delta^*. \tag{5}$$

Closing the loop with plant (1), sensor (2) and controller (3) leads to a relay feedback system (RFS)

$$\text{RFS} \begin{cases} f^+(t) : \dot{x}(t) = Ax(t) + b(\mu + \delta) \\ f^-(t) : \dot{x}(t) = Ax(t) + b(\mu - \delta) \end{cases} . \tag{6}$$

We briefly summarize the properties of the resulting limit cycles for the RFS (6) in the scope of adaptive control here and refer to the literature where possible.

The equilibria x_e^+ of $f^+(t)$ and x_e^- of $f^-(t)$, where $x_e^+ = A^{-1}(-b)(\mu + \delta)$ and $x_e^- = A^{-1}(-b)(\mu - \delta)$, are finite and asymptotically stable under the conditions stated for (1) and for arbitrary μ, $\delta \in \mathbb{R}$. The RFS switches between f^- and f^+ when its trajectory $x(t)$ crosses a switching line

$$S^\pm = \{x \in \mathbb{R} : c^T x = w \mp h\} .$$

When $x(t) \in S^+$, the RFS switches from f^- to f^+ and vice versa for $x(t) \in S^-$. We denote the timespans between the switching instances by t^- and t^+, where f^- applies during t^- and f^+ applies during t^+. The amplitude δ from (3) can be bounded from below as follows.

Lemma 1. (Minimal δ). Consider the RFS in (6) with T, k, h, $\delta \in \mathbb{R}^{>0}$ and w, $\mu \in \mathbb{R}$. A limit cycle establishes with $\mu k \leq w$ for any $\delta > (w + h)k^{-1} - \mu$ and with $\mu k > w$ for any $\delta > (h - w)k^{-1} + \mu$.

See Leonow and Mönnigmann (2019) for the proof of Lemma 1. The lower bound on δ defined by Lemma 1 ensures a repeated switching of the RFS, which is crucial in order not to lose control of the plant. The lower bound on δ depends on the choice of μ and is generally larger than the optimal amplitude δ^*. It follows from Lemma 1 that for the choice of $\mu = wk^{-1}$, the lower bound on δ becomes $\delta \geq (w + h)k^{-1} - \mu = (w + h)k^{-1} - wk^{-1} = hk^{-1}$, which marks the lowest bound on δ with respect to μ that still ensures the switching at $w \pm h$ and therefore coincides with the optimal δ^* as defined in (5). The choice of $\mu = wk^{-1}$ compensates the sensor offset w and is the desired μ^* as defined in (4). It follows that

$$\delta^* = hk^{-1} \text{ for } \mu = \mu^* = wk^{-1} . \tag{7}$$

Lemma 2. (Offset compensation). Assume $u(t) = \mu^* \pm \delta$ with $\mu^* = wk^{-1}$ and $\delta > \delta^*$ is applied to (1). The RFS then converges to a symmetric limit cycle with equal switching timespans $t^+ = t^-$ around the center $x_\mu = A^{-1}(-b)\mu$, where $y_\mu = c^T x_\mu = w$ equals the sensor offset (see Fig. 1).

See Leonow and Mönnigmann (2019) again for the proof of Lemma 2.

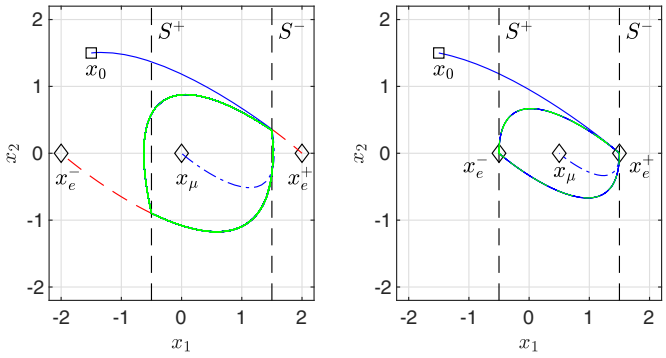

Fig. 1. Trajectories of a sample RFS (6) with $T = 1.1$, $k = 2$, $w = 0.5$, $h = 1$ and initial condition x_0. Parameter values are $\mu = 0$, $\delta = 1$ for the left diagram (i.e., arbitrary initial control, satisfying Lemma 1) and $\mu = \mu^* = 0.25$, $\delta \to \delta^* = 0.5$ for the right diagram (optimal control). The initial trajectory $x(t)$ is depicted in blue, the limit cycle is highlighted in green and the free trajectories of f^+ and f^- (no switching) are marked with a red dashed line. The blue dash-dotted line depicts the trajectory for $\delta = 0$ which approaches the (shifted) origin x_μ.

With parameters μ^* and δ^* from (7), the RFS approaches a limit cycle defined by the set $\Omega \subset \mathbb{R}^n$ of all values of the limit cycle trajectory $x(t)$. If Ω is symmetric, it has a period of $2\tau = 2t^+ = 2t^-$. If the limit cycle is unimodal, i.e., it switches only twice within 2τ, the trajectory starting at $c^T x(t) \in S^+$ evolves towards $c^T x(t + \tau) \in S^-$ and then back to $c^T x(t + 2\tau) = c^T x(t) \in S^+$. Lemma 3 establishes uniqueness and unimodality for Ω.

Lemma 3. (Unique, unimodal limit cycle). Assume that a limit cycle exists for the RFS (6) by choosing μ^* and δ^* as in (7). Then this limit cycle is unique and unimodal.

Proof. Lemmas 1 and 2 already established existence and symmetry of the limit cycle. Colombo et al. (2007) showed unimodality for the regarded class of RFS (6). It remains to show the uniqueness of the limit cycle.

Assume $\mu^* = w = 0$ for simplicity but without loss of generality. The impact map $m^+(x^-) : S^- \to S^+$ maps from a point $x^- \in S^-$ to a point $x^+ \in S^+$ via

$$m^+(x^-) = e^{A\tau(x^-)}x^- + \left(e^{A\tau(x)} - I\right) A^{-1}b\delta$$

(Åström (1995)), where $\tau(x^-)$ is the minimal time that satisfies $m^+(x^-) \in S^+$. The impact map $m^-(x^+) : S^+ \to S^-$ is defined analogously. Combining both maps yields

the Poincaré map $m(x^{\mp}) = m^{\mp}(m^{\pm}(x^{\mp}))$. Assume that $m(\cdot)$ has a fixed point and refer to that fixed point by x^*. $\tau(x^*)$ satisfies $g(\tau(x^*)) = 0$, where

$$g(\tau) = c^T(e^{A\tau} + I)^{-1}(e^{A\tau} - I)A^{-1}b\delta - h \tag{8}$$

(Gonçalves et al., 2000, Gonçalves et al., 2003). Inserting A, b and c^T from (1) into (8) yields

$$g(\tau) = -\frac{2(Th + \delta k\tau)e^{\tau/T} + T((h - \delta k)e^{2\tau/T} + h + \delta k)}{T(e^{\tau/T} + 1)^2} . \tag{9}$$

Setting $\tau = 0$ yields

$$g(0) = -\frac{T(2h + h - \delta k + h + \delta k)}{4T} = -\frac{4Th}{4T} = -h ,$$

which implies $g(0) < 0$ since $h > 0$ by assumption.

The limit $\tau \to \infty$ for $g(\tau)$ from (8) can be found with L'Hospital's rule and $g(\tau) = \frac{g_d(\tau)}{g_n(\tau)}$. This yields

$$\lim_{\tau\to\infty} g(\tau) = \lim_{\tau\to\infty} \frac{g_d^{(4)}}{g_n^{(4)}} = -\frac{(h - \delta k)e^{\tau/T}}{e^{\tau/T}} = -h + \delta k ,$$

which implies $\lim_{\tau\to\infty} g(\tau) > 0$ for $\delta k > h$, which holds according to Lemma 1.

The gradient

$$\frac{\mathrm{d}g(\tau)}{\mathrm{d}\tau} = \frac{2\delta k\tau(e^{\tau/T} - 1)}{T^2(e^{\tau/T} + 1)^3} > 0 \text{ for } \tau \in (0, \infty)$$

$g(\tau)$ is continuous and strictly increasing. Since $g(0) < 0$, $\frac{\mathrm{d}g(\tau)}{\mathrm{d}\tau} > 0$ for all $\tau \in (0, \infty)$ and $\lim_{\tau\to\infty} g(\tau) > 0$, there exists a unique solution to $g(\tau) = 0$ and, consequently, one and only one limit cycle exists for the RFS (6). □

4. SELF-OPTIMIZING CONTROLLER

The computation of the optimal controller parameters μ^* and δ^* can be fully automated so that only minimal user interaction is required. The proposed algorithm exploits the step responses that result naturally when using a binary controller. The resulting control behavior can be described by cycles (see Fig. 2), where each cycle starts at the upper switching point $w + h$ at time t_0, which is detected by the sensor with a binary measurement of $s(t_0) = 1$ according to (2). The controller applies $u(t_0) = \mu - \delta$ (cf. (3)) so that $y(t)$ reaches the lower switching point $w - h$ after the time interval t^-. The sensor output switches to $s(t^-) = 0$ according to (2), which results in a controller output $u(t^-) = \mu + \delta$. After the time t^+, the upper switching point is reached again, marking the end of the cycle.

The step response of (1) with $u(t) = \delta\sigma(t)$, where $\sigma(t)$ is the Heaviside step function, is given by

$$y(t) = k\delta\left(1 - e^{\frac{-t}{T}} - \frac{t}{T}e^{\frac{-t}{T}}\right) + y(0)\left(e^{\frac{-t}{T}} + \frac{t}{T}e^{\frac{-t}{T}}\right) + \dot{y}(0)te^{\frac{-t}{T}} \tag{10}$$

with initial conditions $y(0)$ and $\dot{y}(0)$.

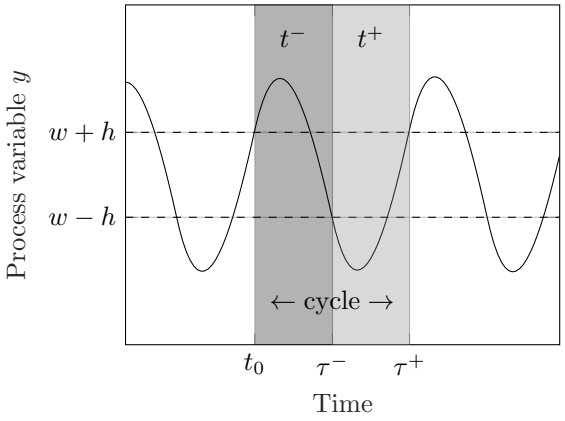

Fig. 2. Definition of one control cycle with descending and ascending parts highlighted illustrating time spans t^- and t^+, respectively

4.1 Computation of μ^*

The mean value μ^* is computed iteratively using the mean value of a cycle given by

$$\tilde{y} = \frac{\int_{t_0}^{\tau^-} y(t)dt + \int_{\tau^-}^{\tau^+} y(t)dt}{t^- + t^+} \tag{11}$$

with $\tau^- = t_0 + t^-$ and $\tau^+ = t_0 + t^- + t^+$. Inserting the process model (1) into (11) and solving the integrals yields

$$\tilde{y} = \frac{k(\mu - \delta)t^- + k(\mu + \delta)t^+ - T^2\left(\dot{y}(\tau^+) - \dot{y}(t_0)\right)}{t^- + t^+}. \tag{12}$$

We assume that $\dot{y}(\tau^+) \approx \dot{y}(t_0)$ for the same cycle, assuming a similar trend of the time derivative of the process variable at the beginning and the end of one cycle. Dividing (12) by k then leads to

$$\tilde{\mu} = \frac{(\mu - \delta)t^- + (\mu + \delta)t^+}{t^- + t^+} , \tag{13}$$

which we claim converges towards μ^* for repeated evaluation of (13).

4.2 Computation of δ^*

If the optimal mean value μ^* and sensor setpoint w are known, the plant gain results from

$$k = \frac{w}{\mu^*} , \tag{14}$$

which can be used further to compute δ^* from (7) with given sensor hysteresis h.

4.3 Computation of T

The time constant of the process is needed for determining the expected time to reach the next sensor switching point. Two subsequent half-cycles with constant $\mu = \mu^*$ but two different amplitudes δ_{r+1} and δ_{r+2} with $\delta_{r+2} < \delta_{r+1}$ are evaluated for the identification of T (see Sec. 4.5 for r). We assume that μ^* has already been found to ensure a symmetric oscillation around the setpoint w according to (4) and (5). We can therefore shift the origin to w to only consider deviations from w and μ^* by choosing $w = 0$

without restriction. Substituting t^+ and t^- into (10) yields

$$\begin{aligned} y(t^+) &= k\delta_{r+1}\left(1 - e^{\frac{-t^+}{T}} - \frac{t^+}{T}e^{\frac{-t^+}{T}}\right) \\ &\quad + y^+(0)\left(e^{\frac{-t^+}{T}} + \frac{t^+}{T}e^{\frac{-t^+}{T}}\right) + \dot{y}^+(0)t^+e^{\frac{-t^+}{T}} \end{aligned} \tag{15a}$$

$$\begin{aligned} y(t^-) &= k\delta_{r+2}\left(1 - e^{\frac{-t^-}{T}} - \frac{t^-}{T}e^{\frac{-t^-}{T}}\right) \\ &\quad + y^-(0)\left(e^{\frac{-t^-}{T}} + \frac{t^-}{T}e^{\frac{-t^-}{T}}\right) + \dot{y}^-(0)t^-e^{\frac{-t^-}{T}} \end{aligned} \tag{15b}$$

with $y^+(0)$ and $y^-(0)$ being the starting conditions for the rising and falling trajectory, respectively. The definition of a cycle as depicted in Fig. 2 for $w = 0$ yields

$$y^-(0) = y(t^+) = h \tag{16}$$

$$y^+(0) = y(t^-) = -h. \tag{17}$$

Since we use two consecutive step responses resulting from different amplitudes δ_{r+1} and δ_{r+2}, the initial condition for the second step response equals the final condition of the first step response. Since δ_{r+2} did not affect the control cycle yet, both initial conditions $\dot{y}^-(0)$ and $\dot{y}^+(0)$ only result from the control with δ_{r+1}. Due to the symmetry of the limit cycle (with μ^* established), the initial conditions for $\dot{y}$ are of the same size with opposite sign, i.e.,

$$\dot{y}^-(0) \approx -\dot{y}^+(0). \tag{18}$$

By substituting (18) in (15a) and (15b) both equations can be transformed to $\dot{y}^-(0)$ or $\dot{y}^+(0)$, respectively. Equating (15a) and (15b) and combining them with relations (16) and (17) then leads to

$$\begin{aligned} &\frac{1}{t^+e^{\frac{-t^+}{T}}}\left[h - k\delta_{r+1}\left(1 - e^{\frac{-t^+}{T}} - \frac{t^+}{T}e^{\frac{-t^+}{T}}\right)\right. \\ &\qquad \left. + h\left(e^{\frac{-t^+}{T}} + \frac{t^+}{T}e^{\frac{-t^+}{T}}\right)\right] \\ &= \frac{1}{t^-e^{\frac{-t^-}{T}}}\left[h - k\delta_{r+2}\left(1 - e^{\frac{-t^-}{T}} - \frac{t^-}{T}e^{\frac{-t^-}{T}}\right)\right. \\ &\qquad \left. + h\left(e^{\frac{-t^-}{T}} + \frac{t^-}{T}e^{\frac{-t^-}{T}}\right)\right], \end{aligned} \tag{19}$$

which can be solved for T numerically.

4.4 Computation of t_p

The predicted timespan t_p for the next control cycle with updated parameters μ and δ results from the step response (10). Substituting t_p for t yields

$$\begin{aligned} y(t_p) &= k\delta^*\left(1 - e^{\frac{-t_p}{T}} - \frac{t_p}{T}e^{\frac{-t_p}{T}}\right) \\ &\quad + y(0)\left(e^{\frac{-t_p}{T}} + \frac{t_p}{T}e^{\frac{-t_p}{T}}\right) + \dot{y}(0)t_pe^{\frac{-t_p}{T}} \end{aligned}$$

with known relations $y(t_p) = \pm h$, $y(0) = \mp h$ for $y(0)$ starting at the lower or upper sensor switching point, respectively. Moreover $\dot{y}(0) \approx 0$ if the optimal amplitude δ^* is used for control. The resulting equation

$$\pm h = k\delta^*\left(1 - e^{\frac{-t_p}{T}} - \frac{t_p}{T}e^{\frac{-t_p}{T}}\right) \mp h\left(e^{\frac{-t_p}{T}} + \frac{t_p}{T}e^{\frac{-t_p}{T}}\right) \tag{20}$$

can be numerically solved for t_p with known T from (19). The proposed algorithm (see Sec. 4.5) uses the predicted time t_p to identify and reject plant disturbances.

4.5 Autonomous parameter identification

The identification of μ^* and δ^* requires $r+2$ control cycles, where $r \in \mathbb{N}^{>0}$ is the number of cycles needed to establish a symmetric oscillation by finding μ^*. Two additional cycles are then required to compute δ^*.

Cycle 0: Initialization The initial cycle controls the plant towards the upper switching point so that $y(t) = w + h$ with $u(t) = \mu_0 + \delta_0$ (see Sec. 4.6 for the choice of the initial parameters μ_0 and δ_0).

Cycles 1 to r: Synchronization The computation of μ^* by (13) is repeated until the time intervals t^- and t^+ are equal, i.e., symmetry of the limit cycle is established.

Cycle r + 1: First step response Cycle $r+1$ uses μ^* and the current amplitude, here denoted by δ_{r+1}.

Cycle r + 2: Second step response Cycle $r+2$ uses μ^* and a reduced $\delta_{r+2} = \rho \cdot \delta_{r+1}$ with $0 < \rho < 1$ to measure a second step response (see Sec. 4.6 for the choice of ρ). After cycle $r+2$ is complete, δ^* is computed using (14) and (7). Subsequently, T is determined by solving (19). T is then used to compute t_p according to (20).

Following cycles: Disturbance rejection The controller updates μ^* at the end of every cycle to compensate minor disturbances. Larger disturbances that prevent the process variable from reaching the sensor switching points result in growing time spans t^- or t^+. The controller continuously evaluates $t^- < 2t_p$ and $t^+ < 2t_p$ and resets its parameters to their initial values μ_0 and δ_0 when $2t_p$ is exceeded to reestablish control of the plant. We update t_p by $t_p = \frac{t^- + t^+}{2}$ after the first full cycle with optimal δ^* to mitigate the effect of inaccuracies in the t_p prediction by (20).

4.6 Notes on the practical implementation

Assuming the optimal parameters μ^* and δ^* are applied to the plant, we can use $\dot{y}(0) \approx 0$. Simplifying (10) by choosing $y(0) = 0$, $u(t) = \mu^* \pm \delta^*$ yields

$$y(t) = k(\mu^* \pm \delta^*)\left(1 - e^{\frac{-t}{T}} - \frac{t}{T}e^{\frac{-t}{T}}\right).$$

For $t \to \infty$ a control with optimal parameters μ^* and δ^* yields $y(t) = w \pm h$. Due to the aperiodic behavior of the plant (1), the switching times approach infinity. This effect is typically mitigated through the process noise. We nevertheless introduce a relaxation factor $\kappa > 1$ according to

$$\delta = \kappa\delta^*$$

to ensure a proper termination of the algorithm also in low noise applications. We found $\kappa = 1.1$ appropriate in a range of applications.

We found that for the second tuning parameter ρ, required for the reduction of δ in cycle $r+2$ as described in Sec. 4.5.4, a choice of $\rho = 0.7$ is appropriate. However, a small gain margin, with δk only marginally greater than h, could

require a larger ρ to prevent δ_{r+2} from being smaller than the minimal amplitude δ^*, thus violating Lemma 1.

A valid choice for the initial controller parameters μ_0 and δ_0 involves spanning the admissible input range of $u(t)$ by applying (3). In many practical applications actuator signals span from 0V to 10V, which leads to $\mu_0 = \delta_0 = 5$V.

5. RESULTS

The proposed controller is demonstrated with the hydraulic test stand depicted in Fig. 3. We used a centrifugal pump (KSB Etanorm G32-125.1) to transfer water from a reservoir (tank 1 in Fig. 3) to an overhead water tank (tank 2 in Fig. 3). The pump features a variable speed drive, the drive speed is proportional to the controller output $u(t)$. An adjustable discharge valve is used to simulate changing process parameters and is set to 80% opening by default.

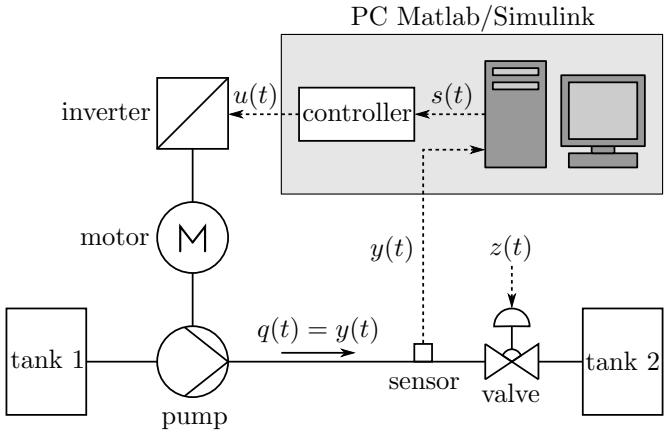

Fig. 3. Test stand used for the evaluation of the adaptive binary controller

The process variable $y(t)$ equals the measured flow $q(t)$ in the hydraulic system. We stress that $y(t)$ is measured continuously only for validation. The adaptive controller is implemented in Matlab/Simulink and receives the binary information $s(t)$ only, here with $w = 40$ L/min and $h = 2$ L/min. After a time of 120 seconds, an external disturbance is introduced by closing the discharge valve to 60%, causing an increased hydraulic resistance. The inputs and outputs of the system are recorded and shown in Fig. 4.

The resulting upper and lower sensor switching points are highlighted by dashed lines in Fig. 4. Furthermore, the upper diagram includes the process variable $y(t)$. The lower diagram shows the controller output $0\% < u(t) < 100\%$ (corresponding to 600 rpm to 1500 rpm pump speed), which is composed of the mean value $\mu(t)$ and the amplitude $\delta(t)$ according to (3).

The initial cycle is performed with parameters $\mu_0 = 50\%$ and $\delta_0 = 50\%$ in order to bring the process variable into the sensor range. At about 5 seconds, the first cycle starts with $\mu_1 = \mu_0$, $\delta_1 = \delta_0$ and applies $u = \mu_1 - \delta_1$ until $y(t)$ reaches the lower switching point $w - h$. The controller then applies $u = \mu_1 + \delta_1$ and the first cycle ends at about 15 seconds with $y(t) = w + h$ crossing the upper switching point. The controller recorded the time spans t^- and t^+ and uses them to compute an updated μ_2, which is closer to μ^* than μ_1. Due to plant-model-mismatch, further cycles are required to find μ^*. The amplitude δ_1 is updated to δ_2 to prevent a violation of the input constraints $\mu \pm \delta \in (0, 100)$ due to the new $\mu_2 \neq \mu_0$. The synchronization cycle is repeated until μ has reached μ^*, which is indicated by $t^+ = t^-$. In the timeseries in Fig. 4, μ^* is found after cycle $r = 5$, i.e., after about 45 seconds. Cycle $r+1$ is then performed with the previously computed μ^* and the current $\delta = \delta_{r+1}$. Cycle $r+1$ ends at about 55 seconds. Cycle $r+2$ uses μ^* and $\delta_{r+2} = \rho \cdot \delta_{r+1}$ and ends at about 65 seconds. At the end of cycle $r+2$, the optimal amplitude δ^* is computed as described in Sec. 4.5.4 and applied for the following cycles. The controller now operates in its optimal setting and compensates minor disturbances (e.g., process noise) by updating μ^* at the end of every cycle.

At 120 seconds, the forced external disturbance with reduced discharge valve opening prevents $y(t)$ from reaching the switching point $w + h$. At about 130 seconds (right edge of the first grey area in Fig. 4), the disturbance is detected as the timespan t^+ exceeds $2t_p$ and a reset of the parameters to μ_0 and δ_0 is performed. The algorithm restarts in cycle 0 and converges to the optimal setting after about 200 seconds, now with increased μ^*, since the discharge valve has a lower opening. It should be stressed that in long-term control applications a reset is only needed if a major disturbance occurs.

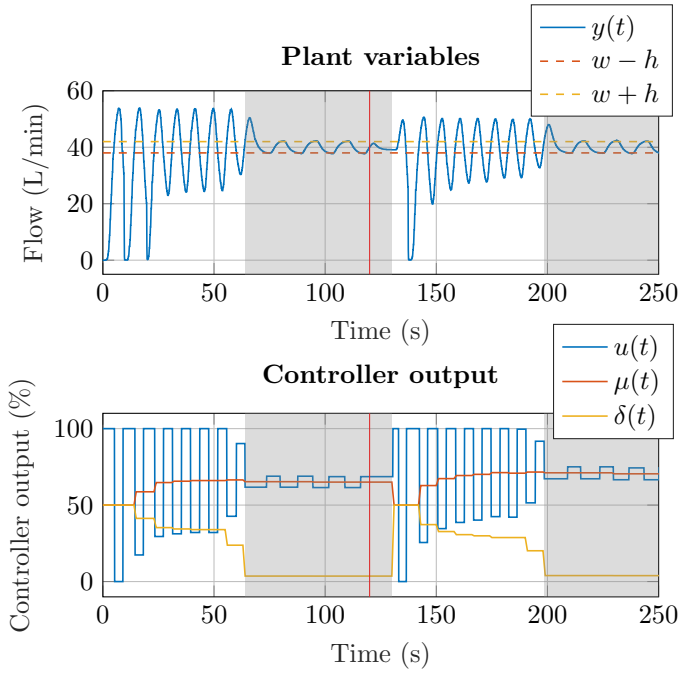

Fig. 4. Time series of test stand data. Grey areas highlight the time intervals the optimal δ^* is used for control. The red vertical line indicates the point in time when the disturbance was introduced.

We compared a simple on/off controller to the proposed adaptive controller and a PID controller in terms of energy demand. The PID controller serves as benchmark here, but requires a more complex continuous measurement of

$y(t)$ in contrast to the binary controllers. The energy demand was evaluated at the described test stand by measuring the electrical power through the inverter. The lower diagram in Fig. 5 shows the accumulated power demand $\int P(t)\mathrm{d}t = E(t)$ for all three controllers for 250 seconds (same measurement run as in Fig. 4). Since the initial parameters μ_0 and δ_0 of the adaptive controller result in an on/off behavior, both controllers show a similar power consumption for the first 20 seconds. As soon as the optimal parameters are computed, the growth of $E(t)$ of the adaptive controller becomes significantly less steep and the gradient of $E(t)$ becomes similar to the one of the PID control. The energy demand of the adaptive controller is reduced by about 30%, compared to the simple on/off controller in the lower diagram. Extrapolating the data to one day of operation (without larger disturbances that would require a reset of the adaptive controller) in the upper diagram of Fig. 5 highlights that the adaptive controller possesses a similar energy efficiency as the PID controller and reduces the energy demand compared to the simple on/off controller even by 50%.

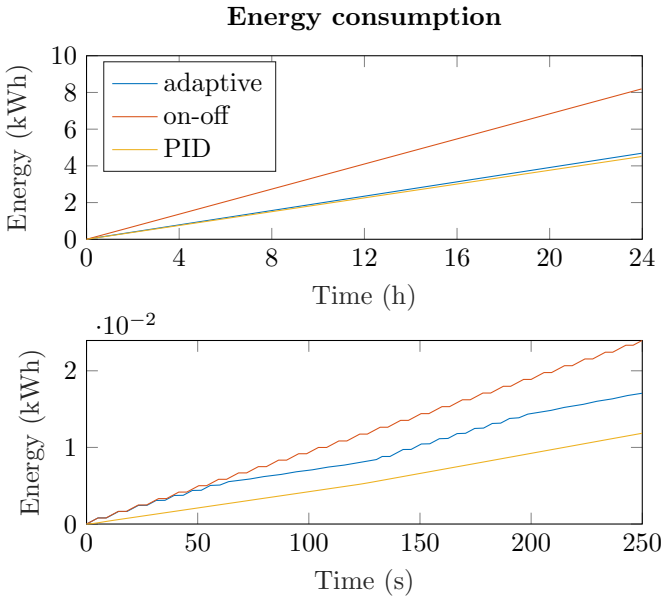

Fig. 5. Comparison of the energy consumption of an on-off, PID and the adaptive controller. The lower diagram correlates with the measurement run from Fig. 4, while the upper diagram depicts an extrapolated operation of the different controllers.

6. CONCLUSION

We proposed a self-optimizing relay feedback controller for an energy efficient control of critically damped second-order systems. Simple binary sensors are sufficient for the proposed algorithm to compute the optimal control parameters in order to minimize the oscillations of the process variable to a minimum. Apart from easy to acquire sensor setpoint and hysteresis, no additional information about the process is needed for the proposed controller to optimize energy consumption and reduce actuator stress.

ACKNOWLEDGEMENTS

This project was supported by funds from the Europäischer Fonds für regionale Entwicklung (EFRE).

EUROPÄISCHE UNION
Investition in unsere Zukunft
Europäischer Fonds
für regionale Entwicklung

REFERENCES

Al-Azba, M., Cen, Z., Remond, Y., and Ahzi, S. (2020). An optimal air-conditioner on-off control scheme under extremely hot weather conditions. *Energies*, 13(5).

Ardalan, S. and Paulos, J. (1987). An analysis of nonlinear behavior in delta-sigma modulators. *IEEE Transactions on Circuits and Systems*, 34(6), 593–603.

Åström, K.J. (1995). Oscillations in systems with relay feedback. In *Adaptive control, filtering, and signal processing*, 1–25. Springer.

Colombo, A., di Bernardo, M., Hogan, S.J., and Kowalczyk, P. (2007). Complex dynamics in a hysteretic relay feedback system with delay. *Journal of Nonlinear Science*, 17(2), 85–108.

da Silva, M. and Barros, P. (2019). A robust relay feedback structure for processes under disturbances: analysis and applications. 1171–1176.

Dietzel, B. and Bek, M. (1996). Digital two-step controller for an actuator element. European Patent EP0894293B1.

Elbert, P., Nüesch, T., Ritter, A., Murgovski, N., and Guzzella, L. (2014). Engine on/off control for the energy management of a serial hybrid electric bus via convex optimization. *IEEE Transactions on Vehicular Technology*, 63(8), 3549–3559.

Feofilov, S.V. and Kozyr, A. (2019). Stability of periodic movements in sampled data relay feedback control systems. In *2019 1st International Conference on Control Systems, Mathematical Modelling, Automation and Energy Efficiency (SUMMA)*, 18–21.

Gonçalves, J.M., Megretski, A., and Dahleh, M.A. (2000). Global stability of relay feedback systems. In *Proceedings of the 2000 American Control Conference*, 6, 220–224.

Gonçalves, J.M., Megretski, A., and Dahleh, M.A. (2003). Global analysis of piecewise linear systems using impact maps and surface Lyapunov functions. *IEEE Transactions on Automatic Control*, 48(12), 2089–2106.

Hetel, L., Fridman, E., and Floquet, T. (2015). Variable structure control with generalized relays: A simple convex optimization approach. *IEEE Transactions on Automatic Control*, 60(2), 497–502.

Juntunen, R.D. (2005). Thermostat relay control. U.S. Patent US7673809B2.

Kang, C.S., Hyun, C.H., and Park, M. (2015). Fuzzy logic-based advanced on–off control for thermal comfort in residential buildings. *Applied Energy*, 155.

Leonow, S., Gunder, T., and Mönnigmann, M. (2019). A self-learning binary controller for energy efficient pump operation. In *Proceedings of the 4th International Rotating Equipment Conference 2019, Wiesbaden*, 1–10.

Leonow, S. and Mönnigmann, M. (2019). A self learning binary controller for increased control performance. In *Proceedings of the 18th European Control Conference 2019, Naples*, 3632–3637.

Levy, S., Korotkin, S., Hadad, K., Ellenbogen, A., Arad, M., and Kadmon, Y. (2012). PID autotuning using relay feedback. In *2012 IEEE 27th Convention of Electrical and Electronics Engineers in Israel*, 1–4.

Li, B. and Alleyne, A.G. (2010). Optimal on-off control of an air conditioning and refrigeration system. In *Proceedings of the 2010 American Control Conference*, 5892–5897.

Michalek, J. (1990). Lernfähiger Zweipunktregler. European Patent EP0455938A1.